eNeuro

Research Article: New Research | Neuronal Excitability

Propagating activity in neocortex, mediated by gap-junctions and modulated by extracellular potassium

https://doi.org/10.1523/ENEURO.0387-19.2020

Cite as: eNeuro 2020; 10.1523/ENEURO.0387-19.2020

Received: 25 September 2019
Revised: 2 January 2020
Accepted: 27 January 2020

Title: Propagating activity in neocortex, mediated by gap-junctions and modulated by extracellular potassium

Abbreviated title: Gap-junction mediated activity in neocortex

List of authors and affiliations:

Christoforos A. Papasavvas[1], R. Ryley Parrish[1], and Andrew J. Trevelyan[1]

1. Institute of Neuroscience, Medical School, Framlington Place, Newcastle upon Tyne, NE2 4HH, UK.

Author Contributions:

CAP and AJT designed research; CAP and RRP performed research; CAP analyzed data; CAP and AJT wrote the paper.

Corresponding author: Andrew J. Trevelyan, andrew.trevelyan@ncl.ac.uk

Number of Figures:	11	**Words for Abstract:**	249
Number of Tables:	1	**Words for Signif. Statement:**	118
Number of Multimedia:	1	**Words for Introduction:**	406
		Words for Discussion:	935

Acknowledgements: The work was supported by project grants from Epilepsy Research UK (P1504) and Medical Research Council (UK) (MR/J013250/1 and MR/R005427/1). AJT was the recipient of a Schaefer Scholarship from Columbia University. CAP was supported by a Wellcome Trust PhD studentship (099755/Z/12/Z).

Conflict of Interest: The authors declare that they have no competing financial interests.

Funding sources:

Medical Research Council (UK)	MR/J013250/1
Medical Research Council (UK)	MR/R005427/1
Epilepsy Research UK	P1504
Wellcome Trust	099755/Z/12/Z

Abstract

Parvalbumin-expressing interneurons in cortical networks are coupled by gap-junctions, forming a syncytium that supports propagating epileptiform discharges, induced by 4-aminopyridine. It remains unclear, however, whether these propagating events occur under more natural states, without pharmacological blockade. In particular, we investigated whether propagation also happens when extracellular K^+ rises, as is known to occur following intense network activity, such as during seizures. We examined how increasing $[K^+]_o$ affects the likelihood of propagating activity away from a site of focal (200-400μm) optogenetic activation of parvalbumin-expressing interneurons. Activity was recorded using a linear 16-electrode array placed along layer V of primary visual cortex. At baseline levels of $[K^+]_o$ (3.5mM), induced activity was recorded only within the illuminated area. However, when $[K^+]_o$ was increased above a threshold level (50^{th} percentile= 8.0mM; interquartile range= 7.5-9.5mM), time-locked, fast-spiking unit activity, indicative of parvalbumin-expressing interneuron firing, was also recorded outside the illuminated area, propagating at 59.1mm/s. The propagating unit activity was unaffected by blockade of GABAergic synaptic transmission, but it was modulated by glutamatergic blockers, and was reduced, and in most cases prevented altogether, by pharmacological blockade of gap-junctions, achieved by any of three different drugs, quinine, mefloquine or carbenoxolone. Wash-out of quinine rapidly re-established the pattern of propagating activity. Computer simulations show qualitative differences between propagating discharges in high $[K^+]_o$ and 4-aminopyridine, arising from differences in the electrotonic effects of these two manipulations. These interneuronal syncytial interactions are likely

to affect the complex electrographic dynamics of seizures, once $[K^+]_o$ is raised above this threshold level.

Significance statement

We demonstrate the spatially extended propagation of activity through a gap-junction mediated syncytium of parvalbumin(PV)-expressing interneurons, in conditions that are known to exist at times within the brain. Previous work has only shown gap-junction coordination very locally, through directly connected cells, or induced at a distance by pharmacological means. We show that cell-class specific spread is facilitated by raised extracellular K^+. This is highly pertinent to what happens at the onset of, and during, seizures, when extracellular K^+ can rise rapidly to levels well in excess of the measured threshold for propagation. Our data suggests that interneuronal coupling will be enhanced at this time, and this has clear implications for the behaviour of these cells as seizures progress.

Introduction

Cortical interneurons are connected by gap-junctions to other interneurons within the same class (Galarreta & Hestrin, 1999; Gibson *et al.*, 1999; Galarreta & Hestrin, 2001; Amitai *et al.*, 2002; Hestrin & Galarreta, 2005; Juszczak & Swiergiel, 2009), providing a highly specific, excitatory link between these cells. Initial studies showed that gap-junction coupling normalised the voltage difference between two cells and further synchronised their firing with millisecond precision (Galarreta & Hestrin, 1999; Gibson *et al.*, 1999; Bennett & Zukin, 2004; Connors & Long, 2004). These studies, however, only examined very

74 localised sets of interneurons, and the question of how widely this synchronisation spreads
75 remained unexamined.

76 Propagation through this gap-junction coupled network has been observed in one
77 particular pathological condition, in a widely used model of epileptic activity, induced by
78 bathing brain slices in 4-aminopyridine (4-AP) (Szente *et al.*, 2002; Gajda *et al.*, 2003; Gigout
79 *et al.*, 2006a). 4-AP blocks various voltage-dependent K^+ channels, and appears to have a
80 disproportionate effect on the population of fast-spiking interneurons, inducing rhythmic
81 bursting in these cells even in the absence of any glutamatergic drive (Avoli *et al.*, 2002;
82 Bohannon & Hablitz, 2018; Parrish *et al.*, 2018). These epileptiform discharges propagate
83 reliably across brain slices, with a broad and relatively slow wave-front. This though
84 represents a rather specific case, in which the spread of activity through the syncytium is
85 facilitated by two factors related to the K^+ conductance blockade, with cells being
86 depolarised and also electrotonically more compact, and which may not occur *in vivo*. In
87 contrast, we speculated that gap-junction mediated propagation may also be supported by
88 a different change in the neuronal milieu, that has been demonstrated both *in vivo* and *in*
89 *vitro*: namely, the raised extracellular potassium ($[K^+]_o$) associated with extreme levels of
90 neuronal activity. We now show that this is indeed the case, although the pattern of
91 spreading activity differs qualitatively from that seen in 4-AP. We used mice that express
92 channelrhodopsin under the PV promoter, allowing us to stimulate specifically this
93 population of interneurons in a highly focal manner. We then examined the time-locked
94 activity propagating out from this focus of activation. We show that this propagation is
95 sensitive to, but not dependent on, glutamatergic synaptic activity, but it is abolished by any
96 of three different gap-junction blockers. We then explore the differences between the two

patterns of spreading activity, induced either by high $[K^+]_o$ or 4-AP, using an extended, multi-neuron, compartmental model of the interneuronal syncytium.

Methods

Cortical expression of optogenetic proteins

All animal handling and experimentation were done according to the guidelines laid by the UK Home Office and Animals (Scientific Procedures) Act 1986 and approved by the Newcastle University Animal Welfare and Ethical Review Body (AWERB # 545). Cortical channelrhodopsin-2 (ChR2) expression was achieved by using genetically engineered transgenic mice. Brain slices were prepared from first generation cross-breeding of homozygous floxed-channelrhodopsin mice (B6; 129S-Gt(ROSA)26Sortm32(CAG-COP4*H134R/EYFP)Hze/J; Jackson Laboratory, stock number 012569) with homozygous PV-cre mice (B6; 129P2-Pvalbtm1(cre)Arbr/J; Jackson Laboratory, stock number 008069).

Preparation of brain slices

Twenty-five young mice (6-12 weeks old) of either sex were killed to prepare the brain slices. They were first anesthetised using Ketamine (0.3 mL / 30 g) and then perfused with ice-cold sucrose-based artificial cerebrospinal fluid (ACSF: NaHCO3 24mM, KCl 3mM, NaH2PO4 1.25mM, sucrose 227.8mM, glucose 10mM, MgCl2 4mM) before the brain was removed to prepare coronal brain slices (400µm thick). The slices were cut on Leica VT1200 vibratome (Leica Microsystems, Wetzlar, Germany) in ice-cold oxygenated (95% O2/ 5%

CO2) ACSF (NaCl 125mM, NaHCO3 26mM, glucose 10mM, KCl 3.5mM, NaH2PO4 1.26mM, MgCl2 3mM). After cutting, the slices were transferred to an incubation, interface chamber (room temperature) perfused with oxygenated (normal) ACSF (NaCl 125mM, NaHCO3 26mM, glucose 10mM, KCl 3.5mM, NaH2PO4 1.26mM, CaCl2 2mM, MgCl2 1mM) for at least 1 hour before transferring them to a recording interface chamber. In the recording interface chamber, the ACSF used was normal ACSF as above. The ACSF was perfused at 1.5-2.5 ml /min and its temperature was kept at 33-36^{o}C. The concentration of extracellular K+ was systematically increased during the recording by adding KCl to the perfused ACSF.

Extracellular recordings

Multichannel extracellular recordings were collected at 25 kHz unless otherwise stated, using a linear 16-channel-probe configuration (A16x1-2mm-100-177; NeuroNexus; electrode separation, 100µm). This was connected to an ME16-FAI-µPA system and MC-Rack software (Multichannel Systems, Reutlingen). The signals were filtered using an analog high-pass filter with a 300Hz cutoff frequency. Data acquisition was carried out using a 1401-3 Analog-Digital converter (Cambridge Electronic Design, Cambridge) and Spike2 software (Cambridge Electronic Design, Cambridge). The electrode array was placed along layer V in the occipital dorsal area of neocortex, approximately corresponding to primary visual cortex (Dong, 2008). Channelrhodopsin was activated by a 470nm LED, delivering light through a Nikon Plan Fluor 4x objective (NA 0.13), using the patterned illuminator Polygon400 (Mightex Systems, Pleasanton, CA, USA). The system was controlled and the patterns were designed through the PolyScan 2 software from the same company. The light intensity was measured at approximately 2mW/mm^2.

AMPA currents were blocked by bathing in 20µM NBQX (HelloBio) and NMDA currents were blocked using 50µM d-APV (Abcam Biochemicals). $GABA_A$ receptors were blocked by gabazine (20µM). We used three different gap junction blockers, namely Mefloquine (50µM), Quinine (100µM, both from Sigma-Aldrich, Gillingham, UK) and Carbenoxolone (100µM, Tocris Bioscience, Bristol, UK).

Multi-unit Activity analysis

The high-pass filtered signals from multiple electrodes were analyzed to extract features of the multi-unit activity (MUA) at different stages of the experiment. We analyzed channels representing the activity from both inside and outside the stimulation area. We first extracted 120-second epochs from the different experimental stages (e.g., low $[K^+]_o$, high $[K^+]_o$), including 6 stimulation trials (20 seconds cycle, 3s stimulation, 17s rest). For each experimental stage, the 3-second segments of the stimulation trials were extracted to represent the activity during stimulation. The resting (non-stimulated) firing rates for each pharmacological condition were derived from four 3-second segments, two from just prior to each trial, and two from just after. The firing rate (spikes/sec) was calculated independently for all the different segments (a threshold of four standard deviations was used for spike detection). Additionally, we measured the rhythmicity of the MUA by determining the timing of each detected spike in regards to the pulse train of stimulation (period of stimulation pulse = 50ms, 25ms light ON, 25ms light OFF). We counted separately all the detected spikes that occurred during the ON phase of the stimulation in each 3-sec segment. The rhythmicity of the MUA is defined as the ratio between the number of spikes detected during the ON phase over the total number of spikes in the 3-sec segment. Notice that this ratio can range from 0 to 1, with 1 indicating that the spikes have a perfect

rhythmicity which is correlated with the stimulation whereas 0 indicates that they have an anti-correlated rhythmicity. A value of 0.5, on the other hand, indicates the absence of rhythmicity with the spikes being uniformly distribution along the 50ms stimulation period. The MUA rhythmicity was applied for both stimulation and baseline segments. The segments representing activity outside the stimulation area were first shifted circularly for 3ms before the calculation of their rhythmicity to compensate for the minimal delay that is expected for the activity recorded at least 150µm away from the stimulation area.

Statistical evaluation of the effect of stimulation and pharmacological manipulations on the MUA was carried out using non-parametric tests. The Wilcoxon rank sum test and its z-statistic was used to evaluate the effect of stimulation on the baseline MUA activity. The median difference with 95% confidence interval was used to evaluate the effect of the pharmacological manipulations. We used the DABEST package of estimation statistics for the latter case (Ho *et al.*, 2019).

Simulations and software accessibility

The model cell consists of three compartments: one soma (27µm length, 29µm diameter, 1 segment) and two morphologically and biophysically identical dendrites (left and right; 200µm length (Fukuda *et al.*, 2006), 0.8µm diameter (Fukuda & Kosaka, 2003), 10 segments). The interneuron model used in this study is adapted from the biophysically detailed interneuron model from Konstantoudaki *et al.,* 2014 (ModelDB, Accession number: 168310) and can be found in Extended Data 1. The soma is equipped with the following mechanisms: fast Na^+ current, A-type K^+ current, delayed-rectifier K^+ current, slow K^+ current, N-type high-threshold activated Ca^{++} current, hyperpolarization-activated cation current (I_h), fast afterhyperpolarization K^+ current and a Ca^{++} buffering mechanism. The

dendrites are equipped with the following mechanisms: fast Na^+ current, A-type K^+ current, and delayed-rectifier K^+ current. The conductance values used are shown in Table 1. Seventy identical cells are scattered in a virtual slice with dimensions 650 x 150 x 150µm. Thus, the density of the population is approximately 5000 PV interneurons / mm^3, which is close to the density found in layer V of mouse primary visual cortex (Pakan *et al.*, 2016). The cells were randomly connected with gap junctions following the connectivity rule in Fig. 11B. A pair of cells would have a maximum of one gap junction (g_{gap} = 0.3nS; Fukuda *et al.*, 2006; Galarreta & Hestrin, 2002) connecting the right dendrite of the cell on the left with the left dendrite of the cell on the right. The placement of the gap junction along the dendrites was symmetric and was randomly placed with a uniform probability distribution between the closest point possible (considering the distance between the cells) and the full length of the dendrite. For example: two cells with 100µm distance between them could be connected from the 50µm dendritic point away from their soma up to the most distal dendritic point, that is, 200µm away from their soma.

The cells that were located in the leftmost 200µm of the virtual slice were directly stimulated at the soma with a 25ms pulse of 0.55nA amplitude starting at 50ms into the simulation. The speed of propagation is calculated based on the first propagation wave, that is, the first spikes of two specific cells. It is equal to the distance travelled over time between the last cell in the stimulation area and the last cell in the overall propagation. For the results shown in Fig. 11E and 11F, only the first 200 long propagations were considered for the analysis. A long propagation is considered a propagation that reaches the 60^{th} cell or beyond that.

All simulations were run using the NEURON simulator (Hines & Carnevale, 2001) through Python (PyNN interface (Davison *et al.*, 2008)). A PC running Ubuntu 16.04 LTS was

used for the simulations. The code for the simulations described in the paper is freely available online at https://github.com/cpapasavvas/PVsynsytium. The code is available as Extended Data 1.

Results

Optogenetic activation of parvalbumin-expressing cells

We investigated the propagation of activity through the syncytium of PV-expressing interneurons, in occipital cortical brain slices in different levels of extracellular K^+. Extracellular recordings were made from 53 mouse brain slices prepared from 22 young adult mice which expressed ChR2 under the PV promoter. We recorded extracellular field potentials using a linear multi-electrode array (MEA; 1.5mm wide array of 16 electrodes with 0.1mm spacing between the shafts) placed along layer V (Fig. 1B), where there is a dense network of electrically coupled PV-expressing interneurons (Galarreta & Hestrin, 1999; Gibson *et al.*, 1999; Fukuda & Kosaka, 2003). We used an optogenetic approach to activate only PV-expressing interneurons, in a small and circumscribed area, extending over 3-4 adjacent electrodes, using a focused patterned illuminator (typically 300-400 x 100 µm, see Fig. 1C and Methods). The blue light was delivered as a train of pulses lasting 3s, at 20 Hz frequency with 50% duty cycle, and repeated every 20s. The spread of activity beyond the light spot was assayed using a linear multielectrode array, which typically extended at least 0.7mm beyond the light spot, sampling at 100µm spaces between individual electrodes.

Propagation of activity with increased extracellular K^+

At baseline levels of extracellular K^+ ($[K^+]_o$ = 3.5mM), neuronal spiking was reliably recorded at those electrodes only within the spot of light, or occasionally from electrodes immediately adjacent (50µm from the edge of illumination), presumably from instances where cells had processes extending into the illuminated area. Critically, though, in this baseline condition, we never recorded triggered activity beyond this restricted site. This pattern of spatially restricted, time-locked activity was very stable, when $[K^+]_o$ was kept constant for an extended period (>30mins, n = 3 brain slices, 90 stimulations; Fig. 1D). We then increased $[K^+]_o$, with increments of 1-2mM every 5-10 mins, to investigate how this affected activity patterns. Predictably, this produced a marked increase in spontaneous activity (Korn *et al.*, 1987; Jensen & Yaari, 1997), and additionally, in 45.3% of all brain slices (24 out of 53 brain slices) we also noted bursts of firing in electrodes away from the illumination site (at least 150µm away), that were time-locked, at short latencies, to the pattern of illumination. Notably, this transition happened rapidly, typically within 2mins, after a threshold level of $[K^+]_o$ was reached, and then remained stable thereafter. Thus, the raised extracellular $[K^+]$ facilitated the spread of activity away from the focal site of optogenetic activation (Fig. 2).

The proportion of brain slices that showed propagation away from the point of illumination increased, as $[K^+]_o$ was raised (Fig. 3). Time-locked activity was seen most typically in the nearest electrode (150µm from the edge of illumination), but was found in some cases in electrodes up to 550µm beyond the edge of the illumination site (Fig. 3, inset). In the more distal cases, (>=250µm from illumination edge), the majority of cases (9/10 brain slices) showed apparent skipping of more proximal electrodes (an example of

this is seen in Fig. 4). This we attributed to the sparse distribution of interneurons, and the poor sampling of this population by the electrodes. Considering only those slices which showed propagation, we fitted a sigmoidal curve to this data, to derive the threshold level of $[K^+]_o$ supporting propagation (50% of trials). The threshold was 8.0 +/- 0.15mM (median +/- 95% confidence interval; Interquartile range = 7.5-9.5mM; full range = 4.5-11.5mM).

Propagating activity was sensitive to glutamatergic and gap-junction blockers, but not GABAergic blockers

We hypothesised that the propagating activity spread through gap-junction connections between PV-expressing interneurons. Examining only brain slices that showed clear propagation of activity beyond the illumination site (20 slices), and working at increased $[K^+]_o$ (mean = 8.40mM; range = 4.5-11.5mM), we first blocked glutamatergic currents using antagonists of AMPA and NMDA receptors (20µM NBQX and 50µM D-APV, respectively), to assess what contribution, if any, was made through conventional synaptic excitatory pathways. This also served to reduce the level of spontaneous activity. In a proportion of brain slices (6 out of 20 slices), following the introduction of glutamate blockers, the evoked propagating activity gradually diminished in parallel with the reduction in spontaneous activity, indicating that synaptic excitation may contribute to these events (Figs. 4 and 5). Notably, in these slices, we were able to resurrect the propagating event by further increasing the extracellular K^+ (Fig. 5), indicating that propagation is facilitated by glutamatergic activity within the slice, but is not dependent on it. In the remaining brain slices (14/20 slices), propagation of activity persisted, following glutamatergic blockade, and indeed was more apparent because it existed on a lower level of background activity.

We next assessed the effects of gap-junction blockers. Unfortunately, this class of drug shows off-target effects (Rozental *et al.*, 2001; Srinivas *et al.*, 2001; Cruikshank *et al.*, 2004), so we examined three different gap-junction blockers: mefloquine, quinine and carbenoxolone. In 4 out of 14 recordings, propagation persisted 15 minutes after the application of a gap junction blocker. In the remaining recordings (10/14 recordings = 71.4%), propagating activity was abolished (see typical examples in Figs. 4-6), and all three drugs showed this effect (quinine, n = 3; mefloquine, n = 6; carbenoxolone, n = 1). The example in Fig. 4 shows the effect of quinine, but this pattern appears representative of the other drugs too, illustrating a rapid and marked decrease in both the amplitude and the firing rate of the recorded activity at electrodes away from the illumination site. Importantly, quinine (unlike the other drugs) can be washed out of the bath (Srinivas *et al.*, 2001), and when this was done, propagating activity was rapidly re-established (Fig. 6). When a different gap-junction blocker, mefloquine (see Fig. 5 and 6, right panel), was then applied, this drug also blocked activity propagation. The recording in Fig. 6 further illustrated another principle, that glutamatergic activity did not sustain this pattern of propagation in the absence of gap-junction coupling.

In a separate set of experiments, we tested whether the blockade of $GABA_A$ receptors affected the propagating activity. In 3 out of 7 slices (from 3 additional mice) we recorded time-locked multiunit activity, under conditions of raised $[K^+]_o$, at sites distant from the illumination locus (150-450µm from illumination edge). In all three cases, this activity persisted unchanged when we successively applied first glutamatergic blockers, and then gabazine to block $GABA_A$ receptors. An example trace is shown in Fig. 7.

We collated the data from all brain slices that displayed evidence of propagating unit activity induced by raising $[K^+]_o$ (Figs. 8 and 9). We analyzed the different pharmacological

conditions with respect to the changes in relative activity (Fig. 9A-C) and rhythmicity (a measure of the time-locked pattern in Fig. 9D-F – see Methods sections for further explanation). These analyses show clearly that the propagation is supported in raised $[K^+]_o$, it persists following blockade of chemical neurotransmission, but is sensitive to blockade of electrical transmission via gap-junctions.

Propagation involves primarily fast-spiking cells

Gap junctions in PV-expressing interneurons are believed always to connect only to other PV interneurons (Galarreta & Hestrin, 1999; Hestrin & Galarreta, 2005). We reasoned therefore that analysis of unit spike shapes in the distant electrodes away from the site of stimulation would provide another test of how these events propagate: events that propagate only through gap-junction coupling would show only PV firing at a distance, whereas those that propagate by synaptic means, including glutamatergic or excitatory GABAergic effects would involve a large degree of pyramidal activation. Spiking in PV interneurons has a highly characteristic signature in the extracellular field potential, with narrow spike widths and prominent overshoot, allowing them to be readily distinguished from so-called “regular-spiking” pyramidal cells.

We separated the 20 brain slices that showed extended propagation into three groups: those that were blocked by glutamate blockers (n=6), those that were blocked by gap-junction blockers (n=10), and those that persisted after these pharmacological manipulations (n=4). We analyzed the spike waveform of the propagating activity for all three groups. An amplitude-based spike sorting procedure was applied to filter out any background activity before analyzing the spike waveform of the time-locked propagating activity. Two features were extracted from each spike waveform: its spike width from valley

to peak (measured in ms) and the amplitude ratio between valley and peak (see lower panels in Fig. 10A; Peyrache *et al.*, 2012). These features are typically used to distinguish activity between fast-spiking and regular-spiking cells (Peyrache *et al.*, 2012). Our spike waveform revealed 4 putative regular-spiking cells and 16 that had a fast-spiking waveform across all groups (Fig. 10A).

Notably, in all the brain slices that were blocked by the gap-junction blockers (group 2), the units were invariably fast-spiking. Pyramidal cells are far more populous than PV interneurons, but on the other hand, usually fire at lower rates. If one assumes that these two effects cancel out, and that therefore one has an equal probability of "finding" a fast-spiking interneuron and a regular spiking neuron, then the probability of finding just fast-spiking interneurons in every single case (n = 10) is approximately 0.1%. In spike sorted data from human neocortex, the ratio of regular to fast-spiking cells is about 80:20 (Peyrache *et al.*, 2012), in which case, the probability of our result is orders of magnitude lower. We concluded therefore that finding only fast-spiking neurons, in every brain slice, would only have happened if the propagation were restricted to that cell class, consistent with propagation through the cell-class specific network created by gap-junction coupling.

We then analyzed the activity recorded across the multielectrode array with respect to the pulsed timing of the photostimulation (peri-stimulation spike histograms, Fig. 10B), in order to assess the propagation speed of the travelling wave of activity. The speed was calculated from the average latency of the first spikes at distal electrodes. We restricted our analyses only to those experiments where we had pharmacological confirmation of the involvement of gap-junctions (i.e. those using quinine, mefloquine or carbenoxolone). These had a median propagation speed of 59.1mm/s and a spatial extent of up to 0.55mm (see Fig. 10B inset).

Simulating propagations through the PV-syncytium

The results presented above demonstrate that propagation through the PV-syncytium under conditions of raised extracellular K^+ is qualitatively different from that induced by 4-AP (Louvel *et al.*, 2001; Gigout *et al.*, 2006a; Gigout *et al.*, 2006b). In raised $[K^+]_o$, propagation was significantly faster (59.1mm/s) than in 4-AP (15mm/s) (Gigout *et al.*, 2006a). There were further differences in the characteristics of the local field potential: in 4-AP, activity had a large low frequency component, indicative of synchronous activity of many cells, and a broad wave-front (Louvel *et al.*, 2001; Gigout *et al.*, 2006a; Gigout *et al.*, 2006b). In high $[K^+]_o$, on the other hand, propagation is manifested as unit activity (single action potentials from isolated cells). As such, the spread of activity in raised $[K^+]_o$ is more sparse, and is prone to failures of propagation, as evidence showed by the reduced extent of the propagating activity in this model (up to 0.55mm), compared to 4-AP (> 2mm (Gigout *et al.*, 2006a)).

In order to understand these differences better, we developed simulations of biophysically detailed cells that are connected through gap junctions in a 3-dimensional virtual slice. In particular, we were keen to assess how the difference in the cellular electrotonic properties in the two cases impacted on the spread. In both cases, neurons are depolarised relative to baseline, but for different reasons: in high $[K^+]_o$, because the K^+ reversal potential is relatively depolarised, and in 4-AP, because there is a reduced K^+ conductance. A further difference is that in 4-AP, the blockade of K^+ channels will additionally reduce the membrane conductivity, meaning that neurons are more electrotonically compact, thus further facilitating spread through the gap-junctions.

We modelled each neuron as a simple, three compartment model, with a soma and two 200µm-long dendrites (see Fig. 11A). Seventy of these cells were uniformly scattered in a 3-dimensional virtual slice, and randomly connected through gap junctions located on their dendrites (Fig. 11A-B). Each cell had a 'left' and 'right' dendrite, and its connectivity with the rest of the network was dictated by its location on the x-axis, such that each dendrite only connected to other neurons on that side. This imposed a directionality to the network, so when the left part of the virtual slice is stimulated, the activity propagated from left to right. The cell index for each cell is defined as its rank in the ordered set of cells from left to right (leftmost cell, id = 1; rightmost cell, id = 70). The connectivity matrix in Fig. 11C shows an example of a randomly connected network, that follows the connectivity rule in Fig. 11B, and shows that the leftmost cells do not have a direct connection with the rightmost cells.

Cells located in the leftmost 200µm of the virtual slice were stimulated 50ms after starting the simulation, and the stimulation pulse, delivered directly to their soma, lasted for 25ms. The exact number of cells stimulated varied slightly from simulation to simulation since the scattering of the cells in the virtual slice was random. Simulations were run for each of the three cases: (1) the control case, where the settings are set to default; (2) the high K^+ case, where the extracellular potassium concentration is considered to be raised to 10.5mM, instead of the default 3.5mM, thus changing E_K and also therefore, raising the resting membrane potential, and reducing the effective action potential threshold; and (3) the 4-AP case, where the membrane resistance is five times higher than the default value and the K^+ channels are almost entirely blocked (conductance is set to 2% of their default value). Typical results of these simulations are shown in Fig. 11D for each one of the different cases. The blue regions in the scatter plots represent the temporal and spatial extend of the stimulation. For the control case, only the cells in the stimulation area were

active, and this activity did not spread beyond the stimulation area at all. In the high $[K^+]_o$ case, activity propagated beyond the area of stimulation, but typically failed before the end of the slice (i.e., 70th cell). Furthermore, we found that even within the propagating territory, the wave of activity could skip some neurons, since there are multiple paths across the network. Thus, not every cell participates in the propagation. Interestingly, the propagation did not advance smoothly. Rather, following stimulation, there was a rapid and almost simultaneous activation of a group of cells in the middle of the slice, followed by a delay before the next set of neurons were recruited.

Gap-junction mediated propagation in the 4-AP simulations, though, were qualitatively different. There was a more gradual and slow propagation that reliably reached the end of the slice without failing. The participation of the cells was complete, with few, if any, being skipped during the propagation (median = 100% as opposed to 71.1% for high $[K^+]_o$ simulations; $p << 0.001$, two-sided Wilcoxon rank sum test; Fig. 11F). The distribution of the propagation speeds in 200 simulations for each case is shown in Fig. 11E. The median propagation speed for the high K^+ case is 57.1mm/s. This value is close to what was expected from the experimental results presented above. The median propagation speed of the 4-AP case is significantly lower (33.5mm/s; $p << 0.001$, two-sided Wilcoxon rank sum test) but higher than previous studies (15mm/s) (Gigout *et al.*, 2006a).

Discussion

In these studies, we demonstrate propagating waves of activity within the population of fast-spiking interneurons, extending at distance from the point of onset, at levels of $[K^+]_o$ that are commonly seen during a seizure (Somjen, 2004). Previous work has only shown gap-junction coordination very locally, through directly connected cells (Galarreta & Hestrin,

1999; Gibson *et al.*, 1999). Notably, we were able to identify a threshold level of $[K^+]_o$ around 8mM for this propagating activity pattern; below that, at physiological levels of $[K^+]_o$, activation of PV interneurons remains very focal. Previously, several groups have demonstrated the coordination of interneuronal activation across single gap-junctions (Galarreta & Hestrin, 1999; Gibson *et al.*, 1999), but for more extensive propagation within cortical networks, gap junction-facilitated propagation over extended distances has only been demonstrated using pharmacological manipulation, bathing tissue in 4-AP (Szente *et al.*, 2002; Gajda *et al.*, 2003; Gigout *et al.*, 2006a). This pharmacological manipulation, while of interest, does represent a rather extreme disruption of neocortical interneuron behaviour (Codadu *et al.*, 2019a). Of particular relevance to the present study is that 4-AP makes neurons more electrotonically compact, by blocking a large component of K^+ conductance, and will thus naturally facilitate electrotonic propagation. Our new data is the first to show spatially extended propagation in conditions that are known to occur naturally in the living brain.

Since 4-AP has a disproportionately large effect on the population of parvalbumin-expressing interneurons (Codadu *et al.*, 2019a), we also chose to study the effect of raised $[K^+]_o$ in this same population. Electrical coupling between this population of interneurons is well established (Galarreta & Hestrin, 1999; Gibson *et al.*, 1999), but coupling has also been described for other populations of cortical interneurons (Galarreta & Hestrin, 2001; Hestrin & Galarreta, 2005), and our findings are likely to generalise to these interneuronal populations too.

One notable finding is that the pattern of gap-junction coupled propagation in high $[K^+]_o$, where we see tightly time-locked and rapid propagation of single action potentials, appears different from that in 4-AP, which takes the form of a broad wave-front, with a

relatively small high frequency component (e.g. (Gigout *et al.*, 2006a; Gigout *et al.*, 2006b; Parrish *et al.*, 2018). A further distinction between these two experimental paradigms is that 4-AP waves additionally involve other interneuronal populations, and may also trigger waves of raised $[K^+]_o$ themselves, secondary to GABAergic induced chloride-loading (Viitanen *et al.*, 2010), both of which would be expected to broaden the wave. It is noteworthy therefore that 4-AP also blocks K^+ channels in glia (Hosli *et al.*, 1981), which may boost the transient rise in $[K^+]_o$, an effect which may be further enhanced by gap-junction blockers. The resultant slow transient of $[K^+]_o$ following a protracted burst of interneuronal activity (Viitanen *et al.*, 2010) may also contribute to the broad wave-front in 4-AP.

Extended propagation of activity within the PV population only occurred at raised levels of $[K^+]_o$, but appears also to be boosted by background levels of excitatory neurotransmission. Blockade of glutamatergic neurotransmission led to a failure of propagation in a proportion of brain slices, but interestingly, it was possible to resurrect the propagating events by further raising the bathing $[K^+]_o$. Together these data support the model we present, in which the likelihood of propagation is dictated by level of depolarisation of the cell at rest, which dictates the ease with which the next element in a chain of neurons is recruited, and how electrotonically compact the network is. Both raised $[K^+]_o$ and a tonic level of glutamatergic drive facilitates propagation by the first mechanism, while blocking K^+ conductances using 4-AP facilitates it by making each element more electrotonically compact. It is possible that excitatory GABAergic activity could also facilitate propagation in this same way, although we did not test this explicitly. It is important though that our results are not consistent with propagation solely through excitatory GABAergic effects, because this would lead to non-specific activation of different cell classes, whereas our spike-sorting analyses indicate that in the great majority of cases

464 (and all cases in which propagation was suppressed by gap junction blockers), propagating
465 activity is restricted to the fast-spiking class of interneurons. Thus, any contribution from
466 excitatory GABAergic effects is likely only to be an adjunct to the coupling we observed,
467 rather than the primary means of propagation.

468 The primary effect of enhancing the electrical coupling of interneurons, in this way, will
469 be to extend the inhibitory surround during focal cortical activation (Prince & Wilder, 1967;
470 Schwartz & Bonhoeffer, 2001; Trevelyan *et al.*, 2006; Parrish *et al.*, 2019), while also
471 enhancing coordination of this inhibitory effect. Interneuronal activity at this time,
472 however, is a double edged sword, because there is now good evidence that these neurons
473 may become active drivers of epileptic discharges, if pyramidal cells become loaded with
474 chloride (Huberfeld *et al.*, 2007; Dzhala *et al.*, 2010; Avoli & de Curtis, 2011; Ellender *et al.*,
475 2014; Pallud *et al.*, 2014; Alfonsa *et al.*, 2015; Raimondo *et al.*, 2015; Alfonsa *et al.*, 2016;
476 Chang *et al.*, 2018; Magloire *et al.*, 2019). Raised extracellular K^+ will also facilitate chloride
477 loading, which is coupled via the cation-chloride co-transporter, KCC2. In either case,
478 whether GABAergic output is inhibitory or excitatory, the enhanced coupling of
479 interneurons through their gap-junctions is likely to be an important determinant of the
480 complex pattern of propagating local field potentials during a seizure (Viventi *et al.*, 2011;
481 Smith *et al.*, 2016; Codadu *et al.*, 2019b). It is also highly pertinent that gap-junction
482 expression is commonly increased in epileptic brains (Manjarrez-Marmolejo & Franco-Perez,
483 2016). Whether this is protective, or serves to exacerbate the epileptic condition, remains
484 an open question.
485

References

Alfonsa, H., Lakey, J.H., Lightowlers, R.N. & Trevelyan, A.J. (2016) Cl-out is a novel cooperative optogenetic tool for extruding chloride from neurons. *Nature communications*, **7**, 13495.

Alfonsa, H., Merricks, E.M., Codadu, N.K., Cunningham, M.O., Deisseroth, K., Racca, C. & Trevelyan, A.J. (2015) The contribution of raised intraneuronal chloride to epileptic network activity. *J Neurosci*, **35**, 7715-7726.

Amitai, Y., Gibson, J.R., Beierlein, M., Patrick, S.L., Ho, A.M., Connors, B.W. & Golomb, D. (2002) The spatial dimensions of electrically coupled networks of interneurons in the neocortex. *J Neurosci*, **22**, 4142-4152.

Avoli, M., D'Antuono, M., Louvel, J., Kohling, R., Biagini, G., Pumain, R., D'Arcangelo, G. & Tancredi, V. (2002) Network and pharmacological mechanisms leading to epileptiform synchronization in the limbic system in vitro. *Prog Neurobiol*, **68**, 167-207.

Avoli, M. & de Curtis, M. (2011) GABAergic synchronization in the limbic system and its role in the generation of epileptiform activity. *Prog Neurobiol*, **95**, 104-132.

Bennett, M.V. & Zukin, R.S. (2004) Electrical coupling and neuronal synchronization in the Mammalian brain. *Neuron*, **41**, 495-511.

510 Bohannon, A.S. & Hablitz, J.J. (2018) Optogenetic dissection of roles of specific cortical
511 interneuron subtypes in GABAergic network synchronization. *J Physiol*, **596**, 901-919.
512
513 Chang, M., Dian, J.A., Dufour, S., Wang, L., Moradi Chameh, H., Ramani, M., Zhang, L.,
514 Carlen, P.L., Womelsdorf, T. & Valiante, T.A. (2018) Brief activation of GABAergic
515 interneurons initiates the transition to ictal events through post-inhibitory rebound
516 excitation. *Neurobiol Dis*, **109**, 102-116.
517
518 Codadu, N.K., Graham, R.T., Burman, R.J., Jackson-Taylor, R.T., Raimondo, J.V., Trevelyan,
519 A.J. & Parrish, R.R. (2019a) Divergent paths to seizure-like events.
520 *https://*http://www.biorxiv.org/content/10.1101/641530v1.
521
522 Codadu, N.K., Parrish, R.R. & Trevelyan, A.J. (2019b) Region-specific differences and areal
523 interactions underlying transitions in epileptiform activity. *J Physiol*.
524
525 Connors, B.W. & Long, M.A. (2004) Electrical synapses in the mammalian brain. *Annu Rev*
526 *Neurosci*, **27**, 393-418.
527
528 Cruikshank, S.J., Hopperstad, M., Younger, M., Connors, B.W., Spray, D.C. & Srinivas, M.
529 (2004) Potent block of Cx36 and Cx50 gap junction channels by mefloquine. *Proc Natl*
530 *Acad Sci U S A*, **101**, 12364-12369.
531

Davison, A.P., Bruderle, D., Eppler, J., Kremkow, J., Muller, E., Pecevski, D., Perrinet, L. & Yger, P. (2008) PyNN: A Common Interface for Neuronal Network Simulators. *Frontiers in neuroinformatics*, **2**, 11.

Dong, H.W. (2008) *Allen reference atlas : a digital color brain atlas of the C57Black/6J male mouse*. Wiley, Hoboken, N.J.

Dzhala, V.I., Kuchibhotla, K.V., Glykys, J.C., Kahle, K.T., Swiercz, W.B., Feng, G., Kuner, T., Augustine, G.J., Bacskai, B.J. & Staley, K.J. (2010) Progressive NKCC1-dependent neuronal chloride accumulation during neonatal seizures. *J Neurosci*, **30**, 11745-11761.

Ellender, T.J., Raimondo, J.V., Irkle, A., Lamsa, K.P. & Akerman, C.J. (2014) Excitatory effects of parvalbumin-expressing interneurons maintain hippocampal epileptiform activity via synchronous afterdischarges. *J Neurosci*, **34**, 15208-15222.

Fukuda, T. & Kosaka, T. (2003) Ultrastructural study of gap junctions between dendrites of parvalbumin-containing GABAergic neurons in various neocortical areas of the adult rat. *Neuroscience*, **120**, 5-20.

Gajda, Z., Gyengesi, E., Hermesz, E., Ali, K.S. & Szente, M. (2003) Involvement of gap junctions in the manifestation and control of the duration of seizures in rats in vivo. *Epilepsia*, **44**, 1596-1600.

556 Galarreta, M. & Hestrin, S. (1999) A network of fast-spiking cells in the neocortex connected
557 by electrical synapses. *Nature*, **402**, 72-75.
558
559 Galarreta, M. & Hestrin, S. (2001) Spike transmission and synchrony detection in networks
560 of GABAergic interneurons. *Science*, **292**, 2295-2299.
561
562 Gibson, J.R., Beierlein, M. & Connors, B.W. (1999) Two networks of electrically coupled
563 inhibitory neurons in neocortex. *Nature*, **402**, 75-79.
564
565 Gigout, S., Louvel, J., Kawasaki, H., D'Antuono, M., Armand, V., Kurcewicz, I., Olivier, A.,
566 Laschet, J., Turak, B., Devaux, B., Pumain, R. & Avoli, M. (2006a) Effects of gap
567 junction blockers on human neocortical synchronization. *Neurobiol Dis*, **22**, 496-508.
568
569 Gigout, S., Louvel, J. & Pumain, R. (2006b) Effects in vitro and in vivo of a gap junction
570 blocker on epileptiform activities in a genetic model of absence epilepsy. *Epilepsy*
571 *Res*, **69**, 15-29.
572
573 Hestrin, S. & Galarreta, M. (2005) Electrical synapses define networks of neocortical
574 GABAergic neurons. *Trends Neurosci*, **28**, 304-309.
575
576 Hines, M.L. & Carnevale, N.T. (2001) NEURON: a tool for neuroscientists. *Neuroscientist*, **7**,
577 123-135.
578

579 Ho, J., Tumkaya, T., Aryal, S., Choi, H., & Claridge-Chang, A. (2019) Moving beyond P values:
580 data analysis with estimation graphics. *Nat Methods*, **16**, 565–566
581
582 Hosli, L., Hosli, E., Andres, P.F. & Landolt, H. (1981) Evidence that the depolarization of glial
583 cells by inhibitory amino acids is caused by an efflux of K+ from neurones. *Exp Brain*
584 *Res*, **42**, 43-48.
585
586 Huberfeld, G., Wittner, L., Clemenceau, S., Baulac, M., Kaila, K., Miles, R. & Rivera, C. (2007)
587 Perturbed chloride homeostasis and GABAergic signaling in human temporal lobe
588 epilepsy. *J Neurosci*, **27**, 9866-9873.
589
590 Jensen, M.S. & Yaari, Y. (1997) Role of intrinsic burst firing, potassium accumulation, and
591 electrical coupling in the elevated potassium model of hippocampal epilepsy. *J*
592 *Neurophysiol*, **77**, 1224-1233.
593
594 Juszczak, G.R. & Swiergiel, A.H. (2009) Properties of gap junction blockers and their
595 behavioural, cognitive and electrophysiological effects: animal and human studies.
596 *Prog Neuropsychopharmacol Biol Psychiatry*, **33**, 181-198.
597
598 Korn, S.J., Giacchino, J.L., Chamberlin, N.L. & Dingledine, R. (1987) Epileptiform burst activity
599 induced by potassium in the hippocampus and its regulation by GABA-mediated
600 inhibition. *J Neurophysiol*, **57**, 325-340.
601

602 Louvel, J., Papatheodoropoulos, C., Siniscalchi, A., Kurcewicz, I., Pumain, R., Devaux, B.,
603 Turak, B., Esposito, V., Villemeure, J.G. & Avoli, M. (2001) GABA-mediated
604 synchronization in the human neocortex: elevations in extracellular potassium and
605 presynaptic mechanisms. *Neuroscience*, **105**, 803-813.
606
607 Magloire, V., Cornford, J., Lieb, A., Kullmann, D.M. & Pavlov, I. (2019) KCC2 overexpression
608 prevents the paradoxical seizure-promoting action of somatic inhibition. *Nature*
609 *communications*, **10**, 1225.
610
611 Manjarrez-Marmolejo, J. & Franco-Perez, J. (2016) Gap Junction Blockers: An Overview of
612 their Effects on Induced Seizures in Animal Models. *Current neuropharmacology*, **14**,
613 759-771.
614
615 Pallud, J., Le Van Quyen, M., Bielle, F., Pellegrino, C., Varlet, P., Labussiere, M., Cresto, N.,
616 Dieme, M.J., Baulac, M., Duyckaerts, C., Kourdougli, N., Chazal, G., Devaux, B., Rivera,
617 C., Miles, R., Capelle, L. & Huberfeld, G. (2014) Cortical GABAergic excitation
618 contributes to epileptic activities around human glioma. *Science translational*
619 *medicine*, **6**, 244ra289.
620
621 Parrish, R.R., Codadu, N.K., Racca, C. & Trevelyan, A.J. (2018) Pyramidal cell activity levels
622 affect the polarity of gene transciption changes in interneurons. *J Neurophysiol*, **120**,
623 2358–2367.
624

625 Parrish, R.R., Codadu, N.K., Scott, C.M. & Trevelyan, A.J. (2019) Feedforward inhibition
626 ahead of ictal wavefronts is provided by both parvalbumin and somatostatin
627 expressing interneurons. *J Physiol*.
628
629 Peyrache, A., Dehghani, N., Eskandar, E.N., Madsen, J.R., Anderson, W.S., Donoghue, J.A.,
630 Hochberg, L.R., Halgren, E., Cash, S.S. & Destexhe, A. (2012) Spatiotemporal
631 dynamics of neocortical excitation and inhibition during human sleep. *Proc Natl Acad*
632 *Sci U S A*, **109**, 1731-1736.
633
634 Prince, D.A. & Wilder, B.J. (1967) Control mechanisms in cortical epileptogenic foci.
635 "Surround" inhibition. *Arch Neurol*, **16**, 194-202.
636
637 Raimondo, J.V., Burman, R.J., Katz, A.A. & Akerman, C.J. (2015) Ion dynamics during seizures.
638 *Frontiers in cellular neuroscience*, **9**, 419.
639
640 Rozental, R., Srinivas, M. & Spray, D.C. (2001) How to close a gap junction channel. Efficacies
641 and potencies of uncoupling agents. *Methods in molecular biology*, **154**, 447-476.
642
643 Schwartz, T.H. & Bonhoeffer, T. (2001) In vivo optical mapping of epileptic foci and surround
644 inhibition in ferret cerebral cortex. *Nat Med*, **7**, 1063-1067.
645
646 Smith, E.H., Liou, J.Y., Davis, T.S., Merricks, E.M., Kellis, S.S., Weiss, S.A., Greger, B., House,
647 P.A., McKhann Ii, G.M., Goodman, R.R., Emerson, R.G., Bateman, L.M., Trevelyan, A.J.

& Schevon, C.A. (2016) The ictal wavefront is the spatiotemporal source of discharges during spontaneous human seizures. *Nature communications*, **7**, 11098.

Srinivas, M., Hopperstad, M.G. & Spray, D.C. (2001) Quinine blocks specific gap junction channel subtypes. *Proc Natl Acad Sci U S A*, **98**, 10942-10947.

Szente, M., Gajda, Z., Said Ali, K. & Hermesz, E. (2002) Involvement of electrical coupling in the in vivo ictal epileptiform activity induced by 4-aminopyridine in the neocortex. *Neuroscience*, **115**, 1067-1078.

Trevelyan, A.J., Sussillo, D., Watson, B.O. & Yuste, R. (2006) Modular propagation of epileptiform activity: evidence for an inhibitory veto in neocortex. *J Neurosci*, **26**, 12447-12455.

Viitanen, T., Ruusuvuori, E., Kaila, K. & Voipio, J. (2010) The K+-Cl cotransporter KCC2 promotes GABAergic excitation in the mature rat hippocampus. *J Physiol*, **588**, 1527-1540.

Viventi, J., Kim, D.H., Vigeland, L., Frechette, E.S., Blanco, J.A., Kim, Y.S., Avrin, A.E., Tiruvadi, V.R., Hwang, S.W., Vanleer, A.C., Wulsin, D.F., Davis, K., Gelber, C.E., Palmer, L., Van der Spiegel, J., Wu, J., Xiao, J., Huang, Y., Contreras, D., Rogers, J.A. & Litt, B. (2011) Flexible, foldable, actively multiplexed, high-density electrode array for mapping brain activity in vivo. *Nat Neurosci*, **14**, 1599-1605.

672

673 ## Figure legends

674 **Figure 1. Schematic of the experimental setup and an example of the control experiment.**
675 (A) Extracellular recordings were taken using a 16-electrode linear multi-electrode array
676 (MEA) placed along layer V in a mouse cortical brain slice in which ChR2 was expressed in
677 PV^+ cells. The distance between adjacent electrodes was 100 µm. Photostimulation (blue
678 LED) was delivered using a patterned illuminator through the microscope objective. (B) The
679 recordings were taken from the dorsal area of the slice, targeting the primary visual area.
680 (C) Example of an illumination pattern (4-electrode wide area) which was drawn in the
681 middle of the array using the patterned illuminator software. (D) A typical control
682 experiment during which repeated illumination was delivered for 31 minutes while the
683 extracellular K^+ remained at normal levels. The evoked activity was only seen at electrodes
684 within the illumination area, and there was no propagating activity, a pattern that remained
685 stable for the entire duration of the recording (31 mins).

686 **Figure 2. Propagating activity arising with raised extracellular K^+.** The area around a subset
687 of the electrodes was illuminated (marked with blue) with 3-second long pulse trains (20Hz,
688 50% duty cycle), repeated every 20s. PV^+ cells around these electrodes responded with 4-5
689 spikes per pulse (see zoomed-in traces). After raising the extracellular K^+ concentration
690 (from 3.5mM to 7.5mM), induced activity was recorded in a distant electrode as well
691 (150µm away). The activity recorded outside the illumination area was time-locked to the
692 activity inside that area, albeit with a short delay. Considering that the photostimulated cells
693 are GABAergic in nature, the activity at the distant electrode is hypothesized to propagate

694 through the electrical synapses between PV^+ cells. In 6 out of the first 12 slices, we saw
695 evidence of rebound bursting at the end of the train of optogenetic stimuli – such an
696 example is seen in the right traces (black arrow head). Notably, this bursting
697 characteristically involved regular spiking units, and so differed qualitatively from the unit
698 activity seen in the time-locked bursts (see Fig. 10).

699 **Figure 3. Propagation is facilitated by raised extracellular K^+ and the spatial spread of the**
700 **propagations detected.** The cumulative proportion of detected propagations at different
701 levels of extracellular K^+ concentration. The majority of propagations (16 out of 24, 66.7%)
702 were observed with an increase of the extracellular K^+ up to 8.5mM. The threshold (at the
703 50% point) was calculated at 8.0mM after fitting a sigmoidal function (red dashed curve).
704 Inset shows the distance at which time-locked firing was recorded, including instances at up
705 to 550µm away from stimulation area.

706 **Figure 4. Propagating activity is sensitive to drugs that block glutamatergic receptors and**
707 **also gap-junction blockers.** The underlying mechanisms of the propagating activity were
708 investigated by the application of pharmacological agents. This example is the continuation
709 of the example in Fig. 2. First, the glutamate receptors were blocked by applying NBQX and
710 D-APV (left panel). In this example, the spontaneous activity was decreased but the
711 propagated activity at the distant electrode remained strong. This indicates that glutamate
712 release (e.g., through disinhibition) was not involved in the propagation. Then, the gap
713 junction blocker quinine was applied (right panel). The activity, recorded 250µm away, was
714 gradually suppressed, and eventually silenced altogether, as evident from the decreasing
715 amplitude and spike rate.

716 **Figure 5. Propagating activity is facilitated by, but is not dependent on, glutamatergic**
717 **transmission.** Repeated propagation assays in the same slice under different
718 pharmacological conditions. In this example, we first saw propagation at 4.5mM $[K^+]_o$ but
719 this was suppressed by the addition of glutamatergic blockers (filled arrowheads).
720 Propagating events then resumed once $[K^+]_o$ was increased further to 5.5mM (open
721 arrowheads). The propagating activity was subsequently blocked entirely by mefloquine.

722 **Figure 6. Propagating activity is prevented by multiple different gap-junction blockers.** The
723 propagating activity silenced in Fig. 4 was recovered by washing out the blockers (left
724 panel). Stable propagating activity with increasing amplitude was recovered at the electrode
725 350 µm away. This activity remained strong for several minutes until another gap junction
726 blocker was applied, namely mefloquine (right panel). The propagating activity was once
727 again blocked validating the involvement of gap junctions by using two different blockers.

728 **Figure 7. Blockade of GABA A did not block the propagations.** In an alternative
729 experimental protocol, GABA A receptors were blocked using gabazine after the blockade of
730 the glutamate receptors. The propagating activity outside the stimulation area remained
731 strong and the same qualitative result was found in all 3 slices of this protocol.

732 **Figure 8. Summary plot of the effects of different pharmacological interventions on**
733 **spatial extent of propagating activity.**

734 **Figure 9: Summary plots of the effects of different pharmacological interventions on**
735 **multiunit activity (MUA) outside the stimulation area**. (A) Modulation of the firing rate, by
736 optogenetic stimulation, in different pharmacological conditions. In two recordings, the
737 activity appears to drop significantly during the stimulation. This was actually because these

slices had very high baseline activity, but notably, during the stimulation, the activity became tightly time-locked in the distal electrodes, indicative of a propagating effect, that was not evident in low K^+. (B) Median z-score of firing rate modulation, +/- 95% confidence interval, relative to the baseline condition (3.5mM $[K^+]_o$). (C) Median z-score of firing rate modulation, +/- 95% confidence interval, relative to the previous condition. Note that even though there were instances of glutamatergic blockade reducing the spread, across all recordings, there was no consistent effect, relative to the prior high $[K^+]_o$ condition. (D-F) Equivalent plots showing the modulation of the time-locked rhythmicity in the distant electrodes.

Figure 10. Spike waveform analysis and calculation of propagation speed. (A) The spike waveforms of all 20 pharmacologically manipulated propagations were analyzed in terms of their spike width and their amplitude ratio between valley and peak. Both regular and fast spiking waveforms were observed (see lower panels for average spike examples). Notice that none of the hypothesized gap-junction mediated activity was found to exhibit a regular-spiking waveform (i.e., spike width > 0.55ms). (B) Example analysis of the speed of propagation calculation, for the gap-junction mediated propagations. The spike time histograms from two different electrodes were plotted: one inside the illumination area (close to the border) and one outside the illumination area where propagating activity was detected. The period covered by the histogram matches the period of the illumination (50ms). The first peak in each histogram is marked by asterisk. The propagation speed was directly calculated from the time difference between these peaks and the distance between the respective electrodes. The inset shows the distribution of the calculated propagation

760 speeds (only for propagations blocked by gap junction blockers). It reveals high variability
761 (standard deviation 17.2mm/s) and a median speed of 59.1mm/s.

762 **Figure 11: Simulation of the high K^+ propagation and comparison with the 4-AP**
763 **propagation.** (A) Schematic of the model cell and of the model network of electrically
764 connected cells. The cell has a simple morphology with a soma and two dendrites, one on
765 the left and one on the right. The cells are randomly placed in a 3-dimensional virtual slice
766 and they form a network through gap junctions. The left dendrite for each cell is used to
767 connect it with other cells located on its left whereas the right dendrite is used to connect it
768 with cells on the right. The left side of the network is stimulated and the activity propagates
769 to the right. (B) The probability of connection between two cells is linearly decreased as the
770 distance between them increases. (C) Example of a connectivity matrix of a randomly
771 generated network where the yellow colour indicates a connection. The cell id is derived
772 from the ordering of the cells on the x-axis, from left to right. Notice that the leftmost cells
773 do to have any direct connection with the rightmost cells due to the limited length of their
774 dendrite (200 μm). (D) Typical results of the simulation under three conditions: control, high
775 K^+, and 4-AP. In the control case there is no propagation; only the cells in the stimulation
776 area fire. In the high K^+ case, there is a fast propagation to the right side of the network but
777 not all cells are participating. In the 4-AP case, there is qualitatively different propagation
778 where the speed is lower but almost every cell in the network participates. (E) Distribution
779 of propagation speeds for the high K^+ and 4-AP cases. The propagation under high K^+
780 conditions is significantly faster ($p << 0.001$, two-sided Wilcoxon rank sum test). (F)
781 Distribution of participation percentages for the high K^+ and 4-AP cases. The participation

782 under 4-AP conditions is significantly higher ($p << 0.001$, two-sided Wilcoxon rank sum test).

783 The code is available in Extended Data 1.

784

785 **Table 1: Biophysical mechanisms used in the model and their conductance values**

786 **Extended Data 1: Python code for the simulations shown in Fig. 11**

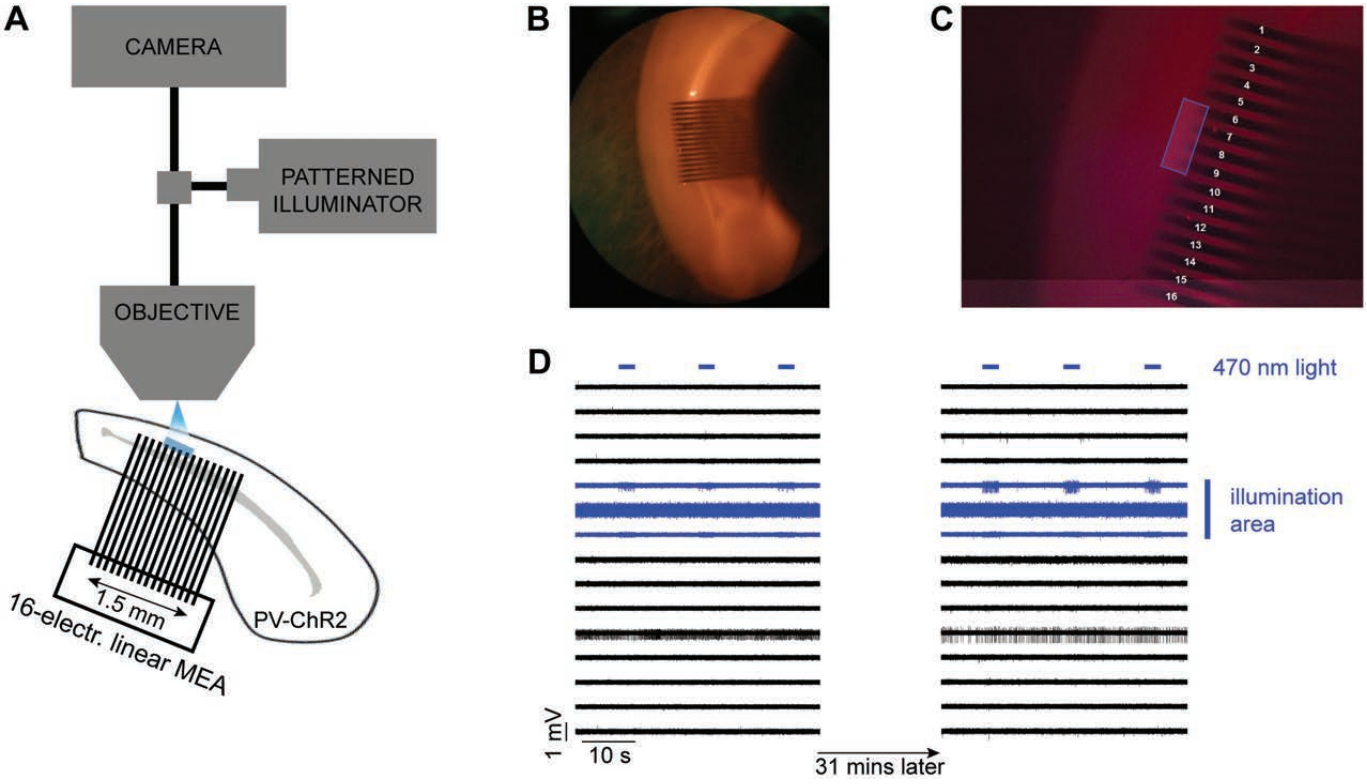

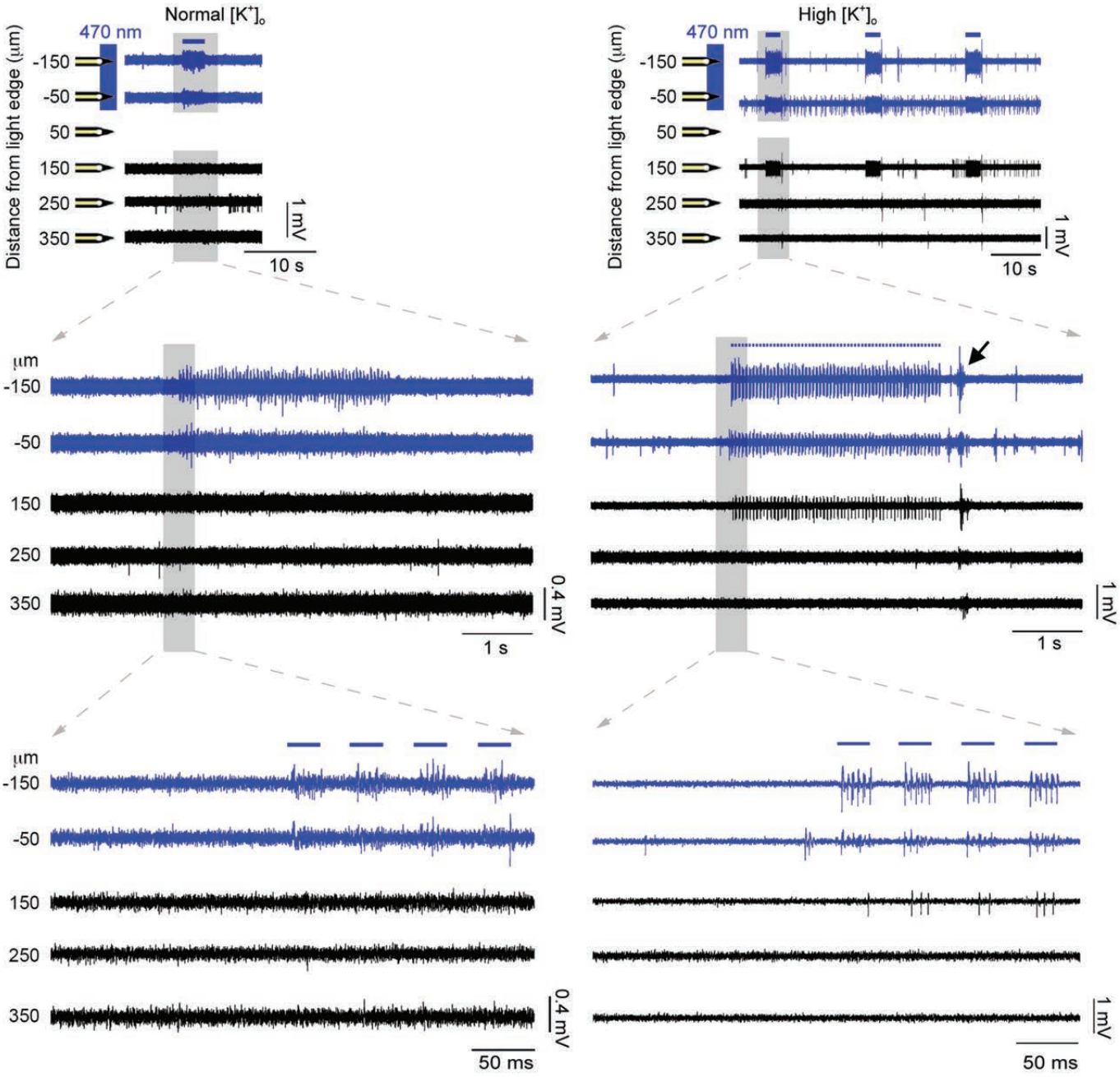

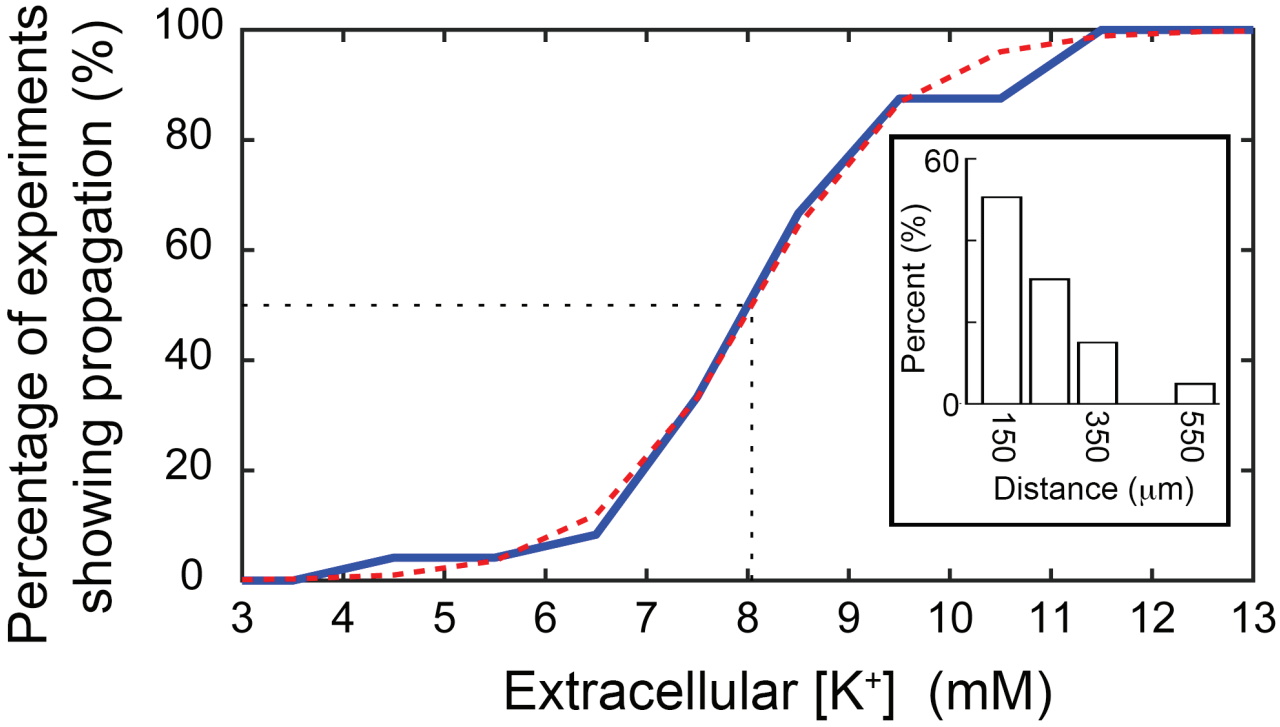

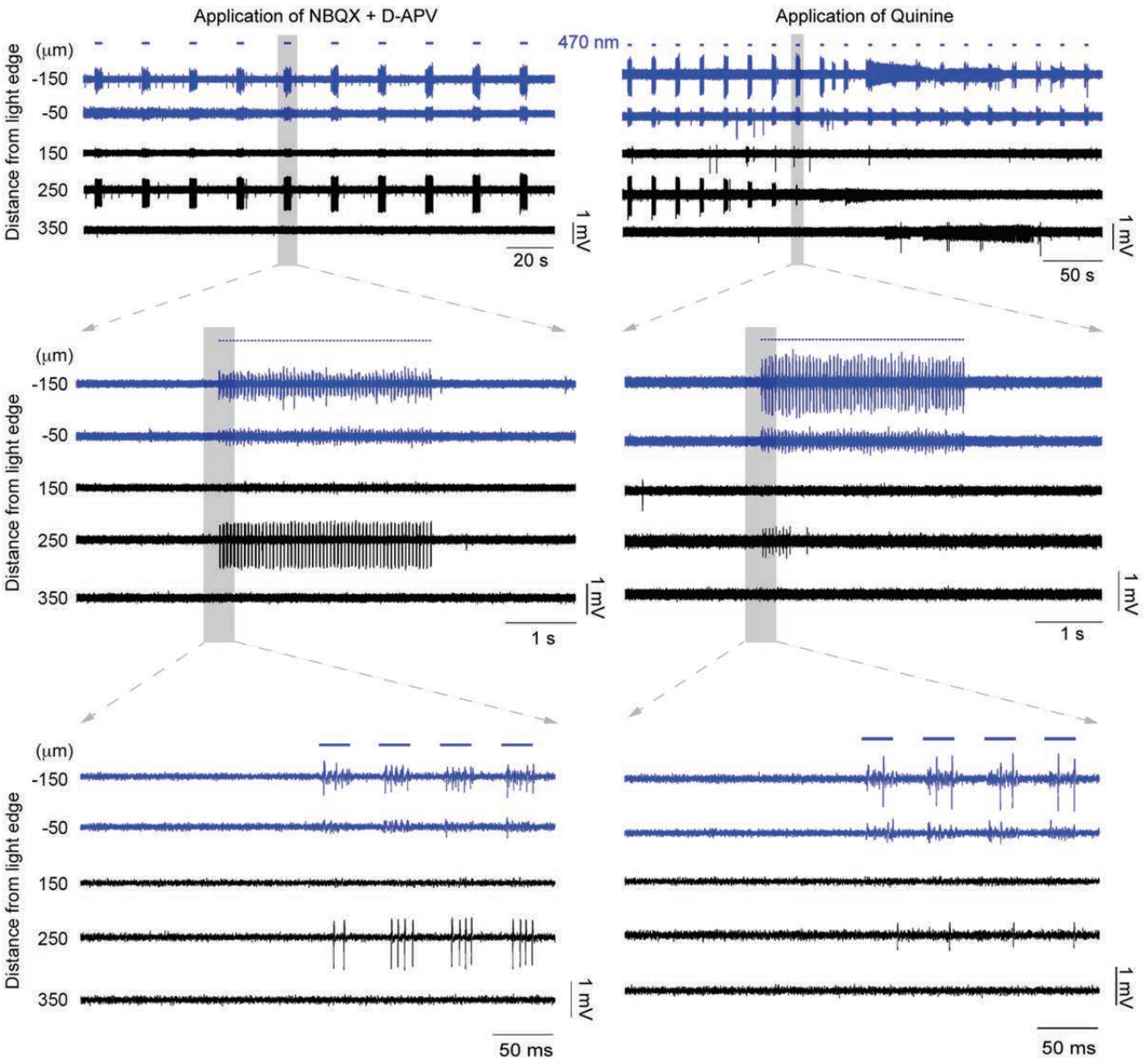

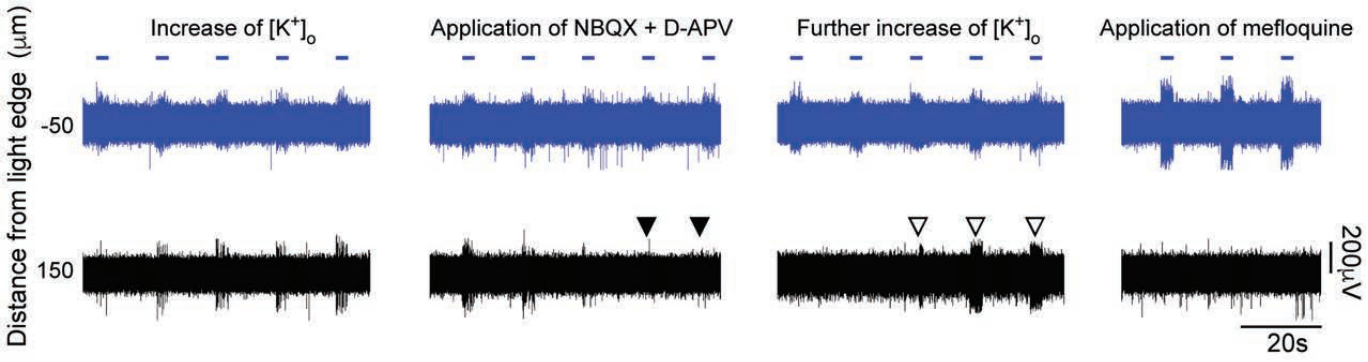

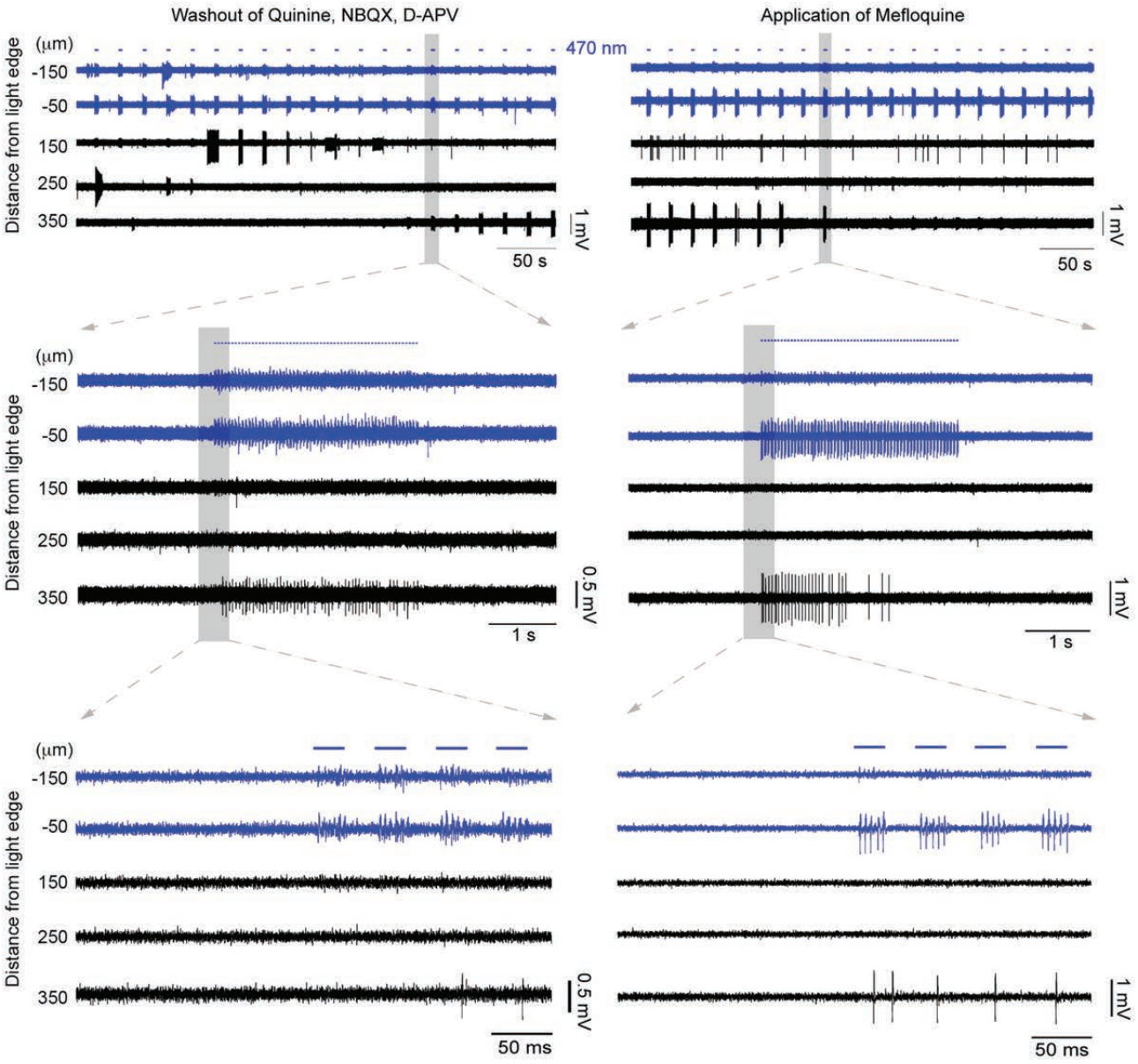

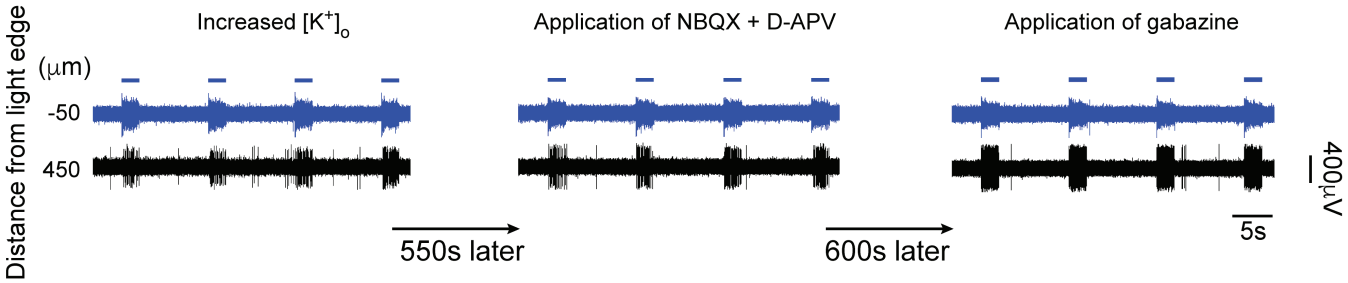

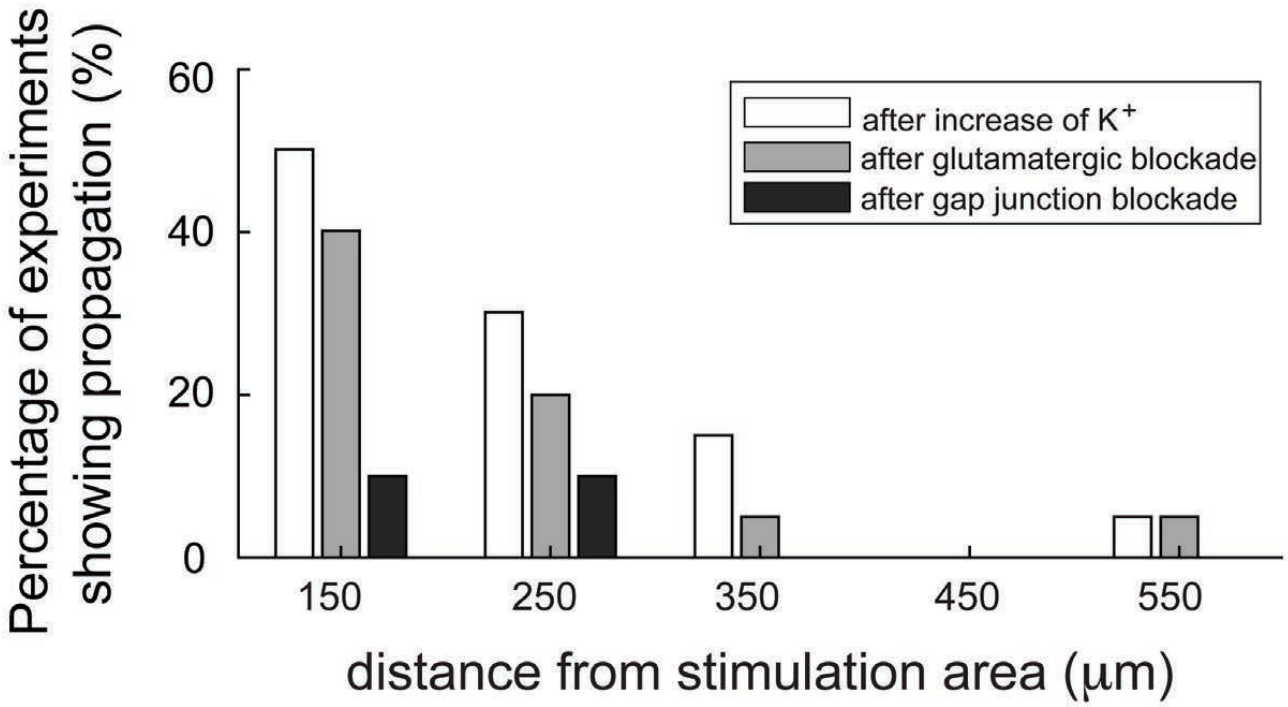

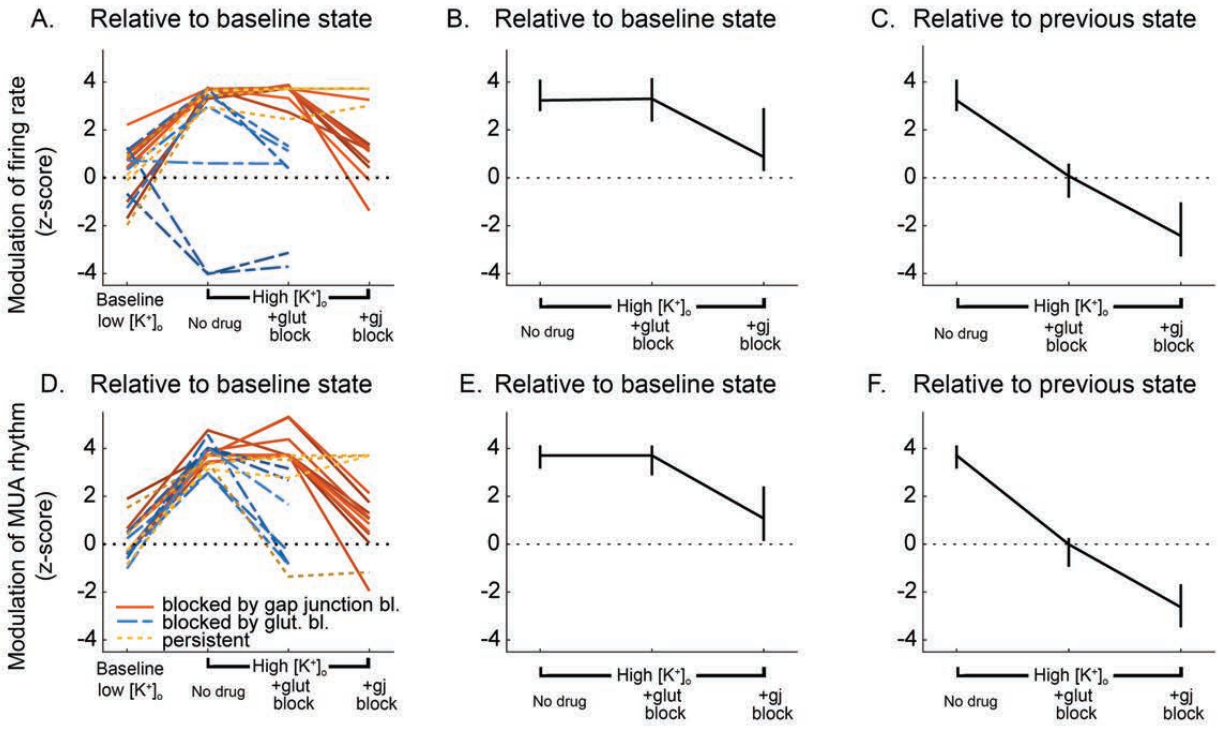

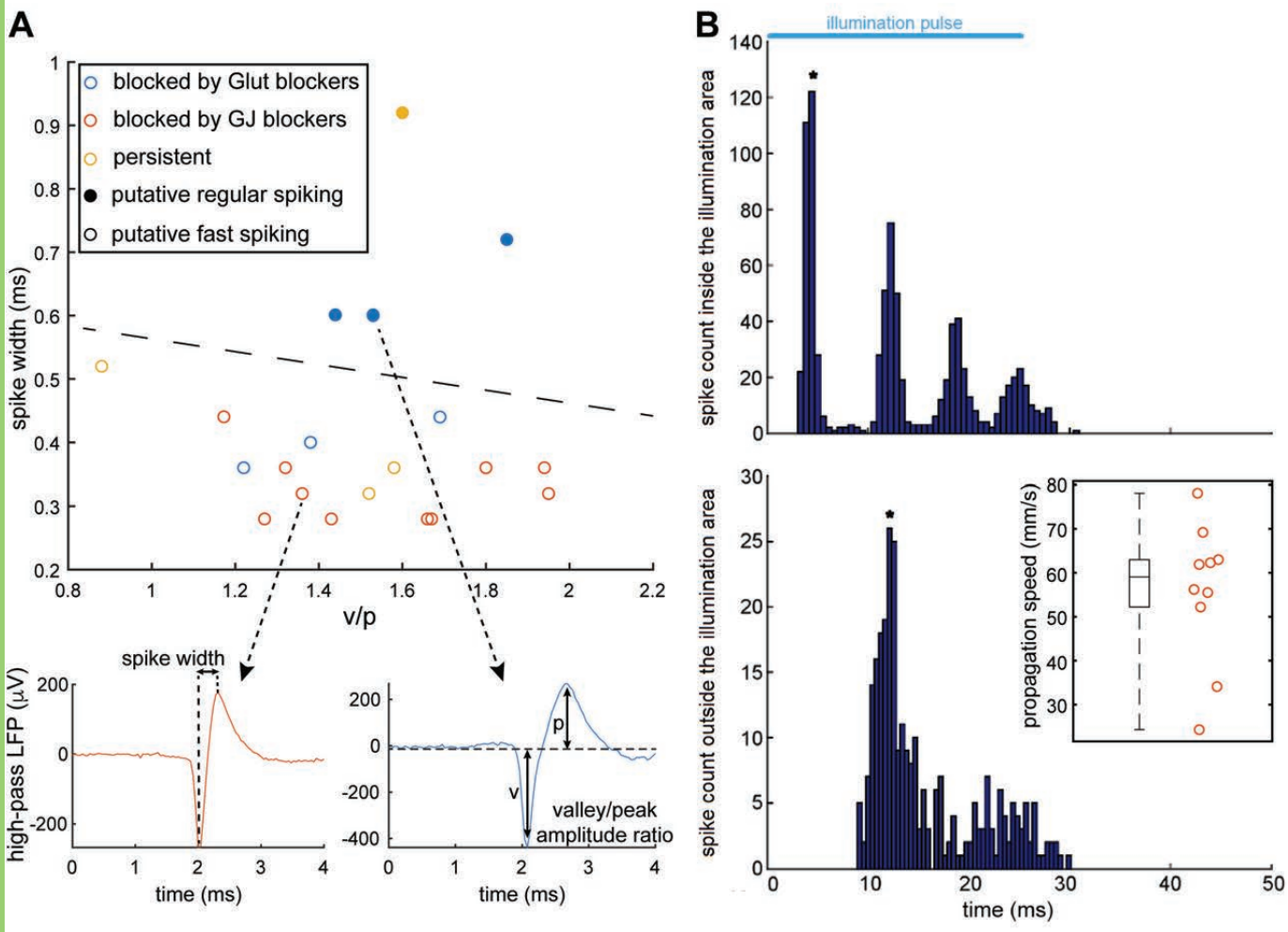

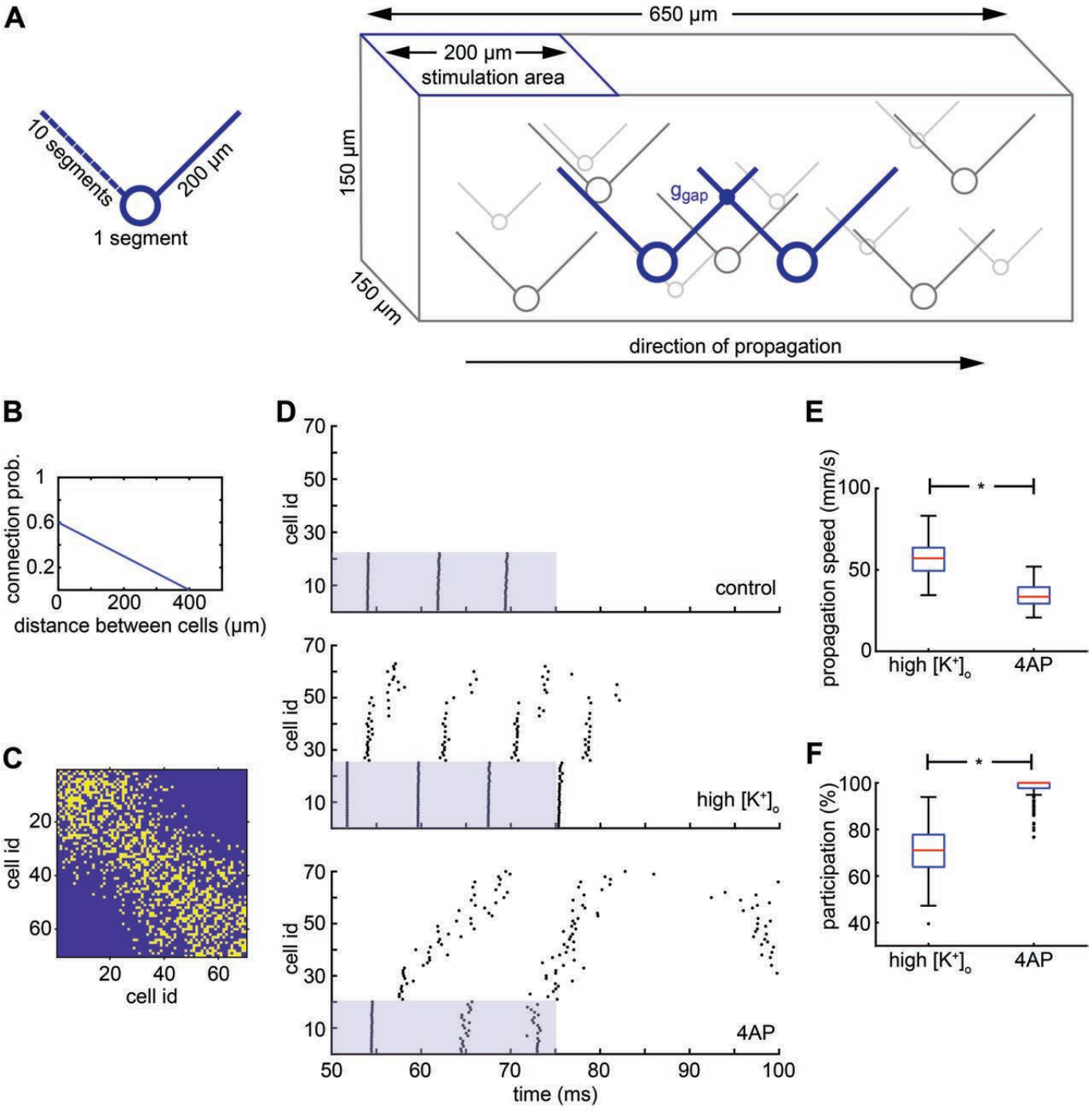

mechanism	soma	dendrite
Na^+ conductance (S/cm^2)	0.045	0.06
Delayed rectifier K^+	0.018	0.009
N-type Ca^{++}	0.0003	N/A
D-type K^+	0.0000725	N/A
H-current	0.00001	N/A
A-type K^+	0.048	0.48
fAHP	0.0001	N/A
Ca^{++} diffusion	yes	no
Cm ($\mu F/cm^2$)	1.2	1.2
Ra (ohm/cm)	150	150
Rm (kOhm cm^2)	10	10